

ECMamba: Consolidating Selective State Space Model with Retinex Guidance for Efficient Multiple Exposure Correction

Wei Dong^{1,*}, Han Zhou^{1,*}, Yulun Zhang², Xiaohong Liu^{2,†}, Jun Chen¹

¹McMaster University ²Shanghai Jiao Tong University
{dongw22, zhouh115, chenjun}@mcmaster.ca yulun100@gmail.com xiaohongliu@sjtu.edu.cn

*Equal Contribution †Corresponding Author

Abstract

Exposure Correction (EC) aims to recover proper exposure conditions for images captured under over-exposure or under-exposure scenarios. While existing deep learning models have shown promising results, few have fully embedded Retinex theory into their architecture, highlighting a gap in current methodologies. Additionally, the balance between high performance and efficiency remains an under-explored problem for exposure correction task. Inspired by Mamba which demonstrates powerful and highly efficient sequence modeling, we introduce a novel framework based on **Mamba** for **Exposure Correction (ECMamba)** with dual pathways, each dedicated to the restoration of reflectance and illumination map, respectively. Specifically, we firstly derive the Retinex theory and we train a Retinex estimator capable of mapping inputs into two intermediary spaces, each approximating the target reflectance and illumination map, respectively. This setup facilitates the refined restoration process of the subsequent **Exposure Correction Mamba Module (ECMM)**. Moreover, we develop a novel **2D Selective State-space layer** guided by **Retinex** information (**Retinex-SS2D**) as the core operator of **ECMM**. This architecture incorporates an innovative 2D scanning strategy based on deformable feature aggregation, thereby enhancing both efficiency and effectiveness. Extensive experiment results and comprehensive ablation studies demonstrate the outstanding performance and the importance of each component of our proposed ECMamba. Code is available at <https://github.com/LowlevelAI/ECMamba>.

1 Introduction

Images captured under over-exposure and under-exposure conditions suffer from various degradations, including reduced contrast, color distortion, and information loss in extremely dark or bright regions. The objective of exposure correction is to enhance the visibility, contrast, and structural details for images with various illumination conditions, which is pivotal for improving the performance of a plethora of downstream applications such as object detection, tracking, and segmentation systems [10, 39, 31] in scenarios with improper exposure.

Similar to other image restoration tasks [3, 2, 32, 25, 26, 23, 42, 12], many deep learning models [38, 6, 34, 44] have been proposed for under-exposed image enhancement and demonstrate commendable results. However, our preliminary experiments indicate that these methods generally perform poorly in multi-exposure correction. This inadequacy stems from the distinct mapping flow between Over-Exposed (OE) and Normal-Exposed (NE) images compared to that between Under-Exposed (UE) and NE images. Recently, some promising works [20, 21, 1, 19] have introduced several interesting deep learning networks to learn consistent exposure representations for multi-exposure correction. However, despite its widespread adoption and outstanding performance in under-exposure correction,

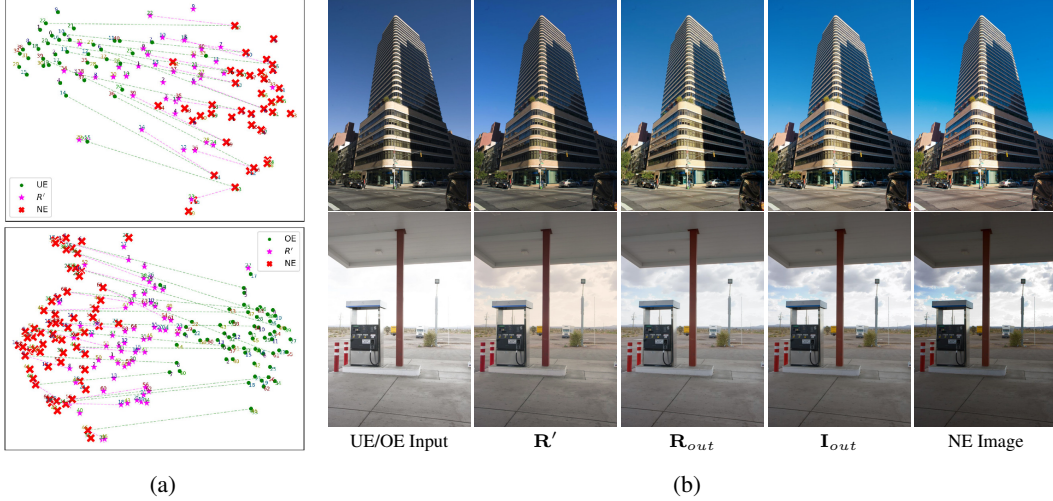


Figure 1: (a) T-SNE [7] visualization of distributions of modulated reflectance (\mathbf{R}'), restored reflectance (\mathbf{R}_{out}) and the final output (\mathbf{I}_{out}) for Under-Exposed (UE) and Over-Exposed (OE) images. Compared to the input data, modulated reflectance (\mathbf{R}') demonstrates closer approximation of Normal-Exposed (NE) images. Besides, compared to the restored reflectance (\mathbf{R}_{out}), our final output (\mathbf{I}_{out}) are better aligned with NE data. (b) Visual result of \mathbf{R}' , \mathbf{R}_{out} and \mathbf{I}_{out} produced by our method. From column 2-4, we observe a noticeable improvement on color preservation and structure recovery, which demonstrates the importance of our introduced two-branch Retinex-based pipeline and the effectiveness of our proposed **ECMamba** network.

Retinex theory [22] has not yet been deeply integrated into deep learning models for multi-exposure correction. As deep learning models often struggle to distinguish between illumination information and the intrinsic reflectance properties of objects in images, simply adopting deep learning models to address such a difficult problem usually obtains sub-optimal results and the incorporation of Retinex theory offers a physically justified way to decompose the illumination and reflectance within deep learning models. Moreover, current state-of-the-art (SOTA) performance is achieved through introducing specific designs (exposure normalization [19] or exposure regularization term [21]) to existing networks. However, these methods present limited generalization, it is essential to develop stronger foundational model with good generalizable ability. Additionally, many methods face a trade-off between performance and efficiency, particularly those based on transformers.

To address these issues, we introduce a novel two-branch Exposure Correction network (**ECMamba**) based on standard **Mamba** architecture, which has demonstrated impressive sequence modeling ability with high efficiency [14]. Specifically, we derive the Retinex theory and develop a Retinex estimator to transform the input into two intermediary spaces, each approximating the target reflectance and illumination map, respectively. As shown in Fig. 1a, compared to the input distribution, the generated intermediary space (\mathbf{R}') shows closer approximation of target distribution, thus enabling subsequent network to execute the fine-grained restoration. Moreover, the visually compelling results in Fig. 1b column 4 demonstrate that our proposed two-branch framework offers more precise estimation and improved performance than simply optimizing the reflectance. Furthermore, we develop a novel **2D Selective State-space** layer guided by **Retinex** information (**Retinex-SS2D**) as the core operator of our **ECMamba**. Different from other scan strategies (*i.e.*, cross-scan mechanism [27]) which considers the scanning of 2D data to 1D sequence a “direction-sensitive” problem, we regard this issue as a “feature-sensitive” problem. Therefore, we first perform feature fusion and then introduce a **Deformable Feature Aggregation (DFA)** guided by Retinex information. Then based on the activation response map derived from DFA, we develop a **Feature-Aware 2D Selective Scanning (FA-SS2D)** mechanism to flatten the aggregated feature into 1D sequence, which is subsequently fed into the standard Selective State Space process (S6) to capture long-range dependencies.

The contributions of this work are summarized as follows:

- ◊ We present a novel **dual-branch framework** that fully embeds **Retinex theory** for exposure correction and we provide detailed explanation for its significance.

◊ By analyzing the operating mechanism of Selective State Space Model, we regard the scanning of vision data is a “**feature-sensitive**” issue and we propose an **efficient Retinex-SS2D layer** with Retinex-guided Feature-Aware 2D Selective Scanning Mechanism.

◊ Extensive experiments and ablations demonstrate the **impressive performance** of our proposed method.

2 Related Works

Learning based Multi-Exposure Correction Multi-exposure correction is a challenging task due to the opposite optimization flows of under-exposure and over-exposure correction. MSEC [1] introduces a Laplacian pyramid architecture to restore lightness and structures. Later, several normalization and regularization methods [4, 21, 19, 20] are proposed for exposure correction. For example, the exposure normalization [19] is proposed for exposure compensation, ECLNet [21] introduces exposure-consistency representations with bilateral activation mechanism, and FECNet [20] opts to correct illumination in the frequency domain. Different from previous methods, we aim to develop a Retinex-based network, where Retinex guidance is utilized to modulating the optimization flows of under-exposure and over-exposure correction.

State Space Model (SSMs) Due to its impressive modeling capability for long-range dependencies and its promising efficiency, State Space Models (SSMs) and recent proposed Structured State-Space Sequence model (S4) [15] has attracted great interests among researchers. Based on S4, several models and strategies are introduced to improve the efficiency and boost the capability, among which Mamba [14] introduces an input-dependent SSM with selective mechanism and achieves superior performance than Transformers for natural language processing. Moreover, some pioneering works have applied Mamba on vision task such as image segmentation [27], classification [47] and even restoration [17, 29]. We are the first to address exposure correction problem based on Mamba, and we innovatively introduce an efficient feature-aware scanning strategy in this work.

3 Preliminaries

State Space Model (S4) State Space Model (S4) is introduced by combining recurrent neural networks (RNNs), convolutional neural networks (CNNs), and classical state space models. Specifically, for a sequence of L length $\mathbf{x} \in \mathbb{R}^L$, the input at any time step $\mathbf{x}(t) \in \mathbb{R}$ can be mapped to an output $\mathbf{y}(t) \in \mathbb{R}$ through the following state space modeling:

$$\begin{aligned} h'(t) &= \mathbf{A}h(t) + \mathbf{B}x(t), \\ y(t) &= \mathbf{C}h(t), \end{aligned} \quad (1)$$

where $\mathbf{h}(t) \in \mathbb{R}^{N \times 1}$ represents latent state and N denotes the dimension scaling ratio in latent state. $\mathbf{A} \in \mathbb{R}^{N \times N}$, $\mathbf{B} \in \mathbb{R}^{N \times 1}$, and $\mathbf{C} \in \mathbb{R}^{1 \times N}$ are state transition matrix, control matrix, and output matrix, respectively. Mathematically, the differential equation in Eq. 1 has an equivalent integral equation and it can be solved using numerical computation. In order to integrating state space modeling into deep learning models, the discretization is required to convert continues-time model to discrete-time system by introducing the timescale $\Delta \in \mathbb{R}$. Specifically, the zero-order hold (ZOH) rule, which is commonly used in SSM-based deep learning algorithms, is applied to transform continuous parameters \mathbf{A}, \mathbf{B} in Eq. 1 to discrete matrix $\bar{\mathbf{A}}, \bar{\mathbf{B}}$ as follows:

$$\begin{aligned} \bar{\mathbf{A}} &= \exp(\Delta \mathbf{A}), \quad \bar{\mathbf{B}} = (\Delta \mathbf{A})^{-1}(\exp(\Delta \mathbf{A}) - \mathbf{I}) \cdot \Delta \mathbf{B}, \\ h(t) &= \bar{\mathbf{A}}h(t-1) + \bar{\mathbf{B}}x(t), \quad y(t) = \mathbf{C}h(t), \end{aligned} \quad (2)$$

where $\bar{\mathbf{A}} \in \mathbb{R}^{N \times N}$, $\bar{\mathbf{B}} \in \mathbb{R}^{N \times 1}$. Moreover, given a sequence with dimension D and length L , the SSM is applied independently to each dimension and $\bar{\mathbf{B}}, \mathbf{C}, \Delta$ are extended with an extra dimension D . The overall computation complexity is $O(LDN)$, which is linear to the sequence length.

Selective State-Space Model (S6) Selective State Space Model is introduced in Mamba with a selective mechanism so that the parameters in SSM can dynamically select necessary information from the context. Specifically, $\bar{\mathbf{B}}, \mathbf{C}, \Delta$ are designed as input-dependent parameters by utilizing linear functions and broadcast operation. This selective mechanism can help Mamba effectively filtering

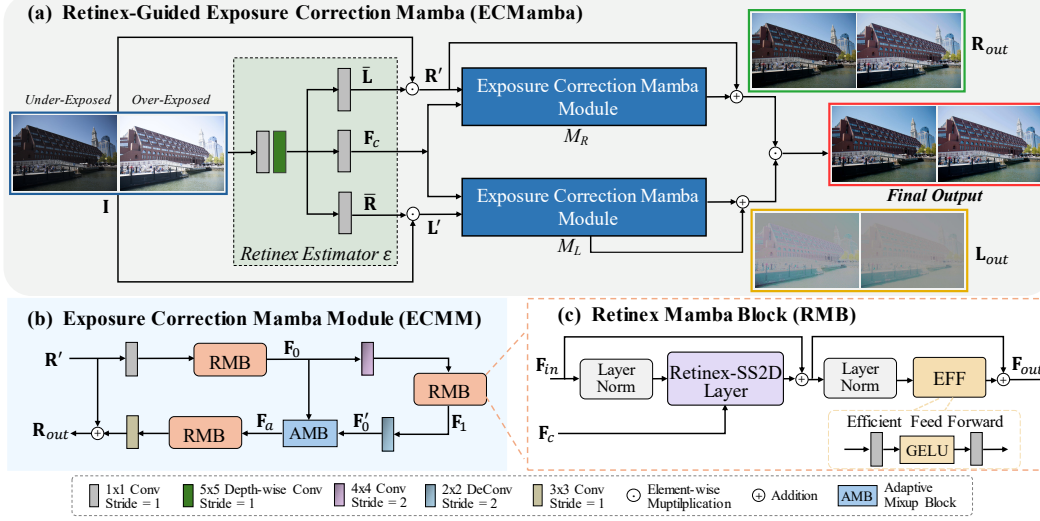


Figure 2: The overall architecture of our proposed Retinex-based framework for exposure correction, which includes a Retinex estimator \mathcal{E} and primary restoration network \mathcal{M}_R and \mathcal{M}_L .

out irrelevant noise and focusing on important tokens, thereby achieving outstanding performances in multiple language and vision tasks.

4 Methodology

The overall framework of our method is shown as Fig. 2, which demonstrate that our proposed exposure correction network is designed based on Mamba and Retinex theory. In this section, we first introduce our formulated Retinex-based Exposure Correction Framework (Sec. 4.1), then we propose to utilize Exposure Correction Mamba Module (ECMM) to achieve precise restoration for the reflectance and illumination map (Sec. 4.2). More importantly, to enhance the efficiency and effectiveness, we introduce a new 2D Selective State-space layer with an innovative scanning mechanism guided by Retinex information (Retinex-SS2D) in Sec. 4.3 and Sec. 4.4.

4.1 Retinex-Guided Exposure Correction Framework

The Retinex theory can be expressed as $I_{GT} = R_{GT} \odot L_{GT}$, where \odot denotes Hadamard product, I_{GT} is an ideal image without degradation, R_{GT} and L_{GT} represent the reflectance image and illumination map, respectively. However, a low-quality image I_{LQ} captured under non-ideal illumination conditions (under-exposure or over-exposure scenes) inevitably suffer from severe noise, color distortion, and constrained contrast. Therefore, we introduce a perturbation to R_{GT} and L_{GT} respectively (\hat{R} and \hat{L}) to model these degraded images as:

$$I_{LQ} = (R_{GT} + \hat{R}) \odot (L_{GT} + \hat{L}) = R_{GT} \odot L_{GT} + R_{GT} \odot \hat{L} + \hat{R} \odot L_{GT} + \hat{R} \odot \hat{L}. \quad (3)$$

Some existing Retinex-based methods [6, 13, 18, 33] regard the reflectance component R_{GT} as the final enhanced result, thus they ignore the last three terms in Eq. 3 and focus on modeling the mapping: $R_{GT} = \mathcal{F}(I_{LQ}) \odot (I_{LQ})$ using network \mathcal{F} . However, these models can only achieve sub-optimal performance due to the difficulty of acquiring accurate mapping, especially for multiple exposure correction task, where multiple Under-Exposed (UE) and Over-Exposed (OE) inputs correspond to one Normal-Exposed (NE) image. Therefore, we choose to restore the reflectance and illumination component simultaneously in order to obtain satisfactory outputs. Specifically, we element-wisely multiply the both sides of Eq. 3 by \bar{L} and \bar{R} respectively as:

$$\begin{aligned} I_{LQ} \odot \bar{L} &= R' = R_{GT} + R_{GT} \odot \hat{L} \odot \bar{L} + \hat{R} + \hat{R} \odot \hat{L} \odot \bar{L}, \\ I_{LQ} \odot \bar{R} &= L' = L_{GT} + \hat{R} \odot L_{GT} \odot \bar{R} + \hat{L} + \hat{L} \odot \hat{L} \odot \bar{R}, \end{aligned} \quad (4)$$

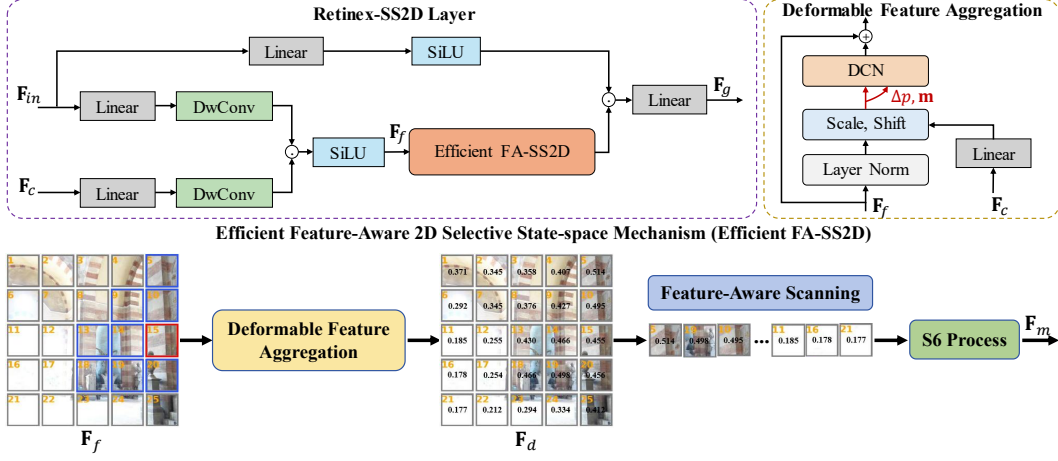


Figure 3: The details of our proposed Retinex-SS2D layer. We firstly fuse the input feature F_{in} and the Retinex guidance F_{in} . Then we propose an innovative Feature-Aware 2D Selective State-space Mechanism, which utilizes Deformable Convolution (DCN) for feature aggregation. Then we propose the feature-aware scanning strategy based on the activation response map derived from DCN. Compared to other 2D scanning methods, our approach generates a sequence ordered by feature importance, thereby maximizing the robust sequence modeling capabilities of Mamba.

where $\bar{\mathbf{L}}$ and $\bar{\mathbf{R}}$ are the matrix such that $\bar{\mathbf{L}} \odot \mathbf{L}_{GT} = \mathbf{1}$ and $\bar{\mathbf{R}} \odot \mathbf{R}_{GT} = \mathbf{1}$, and we assume we can approximate $\bar{\mathbf{L}}$ and $\bar{\mathbf{R}}$ via Retinex estimator \mathcal{E} . $\mathbf{R}_{GT} \odot \hat{\mathbf{L}} \odot \bar{\mathbf{L}} + \hat{\mathbf{R}} \odot \hat{\mathbf{L}} \odot \bar{\mathbf{L}}$ and $\hat{\mathbf{R}} \odot \mathbf{L}_{GT} \odot \bar{\mathbf{R}} + \hat{\mathbf{L}} + \hat{\mathbf{R}} \odot \hat{\mathbf{L}} \odot \bar{\mathbf{R}}$ indicate the remaining degradation in \mathbf{R}' and \mathbf{L}' . Therefore, the well-exposed result can be retrieved using deep-learning networks by

$$(\bar{\mathbf{R}}, \bar{\mathbf{L}}, \mathbf{F}_c) = \mathcal{E}(\mathbf{I}_{LQ}), \quad \mathbf{R}' = \mathbf{I}_{LQ} \odot \bar{\mathbf{L}}, \quad \mathbf{L}' = \mathbf{I}_{LQ} \odot \bar{\mathbf{R}}, \quad (5)$$

$$\mathbf{R}_{out} = \mathbf{R}' + \mathcal{M}_R(\mathbf{R}'; \mathbf{F}_c), \quad \mathbf{L}_{out} = \mathbf{L}' + \mathcal{M}_L(\mathbf{L}'; \mathbf{F}_c), \quad \mathbf{I}_{out} = \mathbf{R}_{out} \odot \mathbf{L}_{out},$$

where \mathcal{M}_R and \mathcal{M}_L are networks utilized to predict the minus degradation in \mathbf{R}' and \mathbf{L}' , and \mathbf{F}_c serves as a Retinex guidance information derived from the \mathbf{I}_{LQ} .

As shown in Fig. 2, the Retinex estimator \mathcal{E} takes \mathbf{I}_{LQ} and its mean matrix along the channel dimension (which is omitted for clarity in Fig. 2) as inputs. \mathcal{E} firstly utilizes a 1×1 convolution and a depth-wise convolution with 5×5 kernel to extract features. Then, $\bar{\mathbf{L}}$, $\bar{\mathbf{R}}$ and \mathbf{F}_c are generated by one 1×1 convolution, respectively. More importantly, \mathbf{R}' and \mathbf{L}' are fed into \mathcal{M}_R and \mathcal{M}_L for further restoration. In addition to optimizing \mathbf{I}_{out} to approximate \mathbf{I}_{GT} , our training objective incorporates a constraint on $\bar{\mathbf{L}}$ and $\bar{\mathbf{R}}$, as discussed in Sec 4.5.

Discussion (i) Many Retinex-based methods [37] aims to learn the mapping between the input and the reflectance image and illumination map, then obtain the final result using Hadamard product operation. However, this strategy is not suitable for multi-exposure correction task. Fig. 1a illustrates the complicated and distant distribution patterns of OE and UE images relative to their normally exposed equivalents. Such complex distributions challenge the establishment of accurate mappings from inputs. However, by carefully analyzing Retinex theory, we construct an intermediary space that significantly reduces the distance to our optimization objectives and facilitates the subsequent fine-tuning restoration process, as shown in Fig. 1b. (ii) Some methods [6, 13, 33, 18] treat \mathbf{R}_{GT} as the final enhanced result, which deviates from the original explanation of Retinex theory and leads to limited performance. Therefore, we adopt a two-branch framework to reconstruct the reflectance and illumination map using distinct deep learning networks. The significance of our framework is discussed in the ablation study (Sec. 5.3).

4.2 Exposure Correction Mamba Module (ECMM)

Together with our proposed Retinex-guided exposure correction framework, we also develop innovative networks that serves as \mathcal{M}_R and \mathcal{M}_L in Eq. 5 to estimate the remaining corruption in \mathbf{R}' and \mathbf{L}' . In order to develop an effective and efficient module that is capable to achieve high performance and

is friendly to resource-limited devices, we propose an novel Retinex-guided Exposure Correction **Mamba Module (ECMM)** which succeeds the powerful modeling capability of Mamba. Notably, \mathcal{M}_R and \mathcal{M}_L shares similar structure and we discuss the details of \mathcal{M}_R in this section.

As illustrated in Fig. 2, our ECMM adopts a two-scale U-Net architecture. For the encoding process, the input \mathbf{R}' is firstly processed by a $\text{conv } 3 \times 3$ and one **RetinexMamba Block (RMB)** to generate the initial feature \mathbf{F}_0 . Then the downsampling operation is achieved by one 4×4 convolution with stride 2, and the down-sampled feature is fed into another RMB to obtain the middle feature \mathbf{F}_1 . For the decoding stage, \mathbf{F}_1 is firstly up-scaled to \mathbf{F}'_0 by a 2×2 deconv with stride 2. To alleviate the information loss caused by the down-sampling process, we introduce an adaptive mix-up feature fusion [46] to transfer the encoding information to the decoder stage as:

$$\mathbf{F}_a = \sigma(\theta)\mathbf{F}_0 + (1 - \sigma(\theta))\mathbf{F}'_0, \quad (6)$$

where θ represents a learnable coefficient, and σ denotes the sigmoid function. Then the fused feature \mathbf{F}_a is fed into the RMB and the convolution layer sequentially and the restored reflectance \mathbf{R}_{out} is obtained by a residual addition according to Eq. 5.

4.3 RetinexMamba Block (RMB)

As the core operator to extract and aggregate features in ECMM, our RMB block adopts a similar architecture with Transformer block. However, the significant computational demands of self-attention and cross-attention mechanisms obviously compromise the efficiency of Transformer-based methods, precluding their application in real-time or resource-constrained environments. To this end, we remove the attention process and introduce an innovative **Retinex-guided 2D Selective State-space (Retinex-SS2D)** layer to capture long-range dependencies and facilitate dynamic feature aggregation. Therefore, the feature flow of our RMB can be described as:

$$\mathbf{F}'_{out} = \mathbf{F}_{in} + \text{Retinex-SS2D}(\text{LN}(\mathbf{F}_{in}), \mathbf{F}_c), \quad \mathbf{F}_{out} = \mathbf{F}'_{out} + \text{EFF}(\text{LN}(\mathbf{F}'_{out})), \quad (7)$$

where LN denotes the LayerNorm, \mathbf{F}_{in} and \mathbf{F}_{out} represent the input and output feature of RMB. \mathbf{F}_c is the Retinex guidance information extract by the Retinex estimator \mathcal{E} . Moreover, inspired by ConvNext [28, 8], we remove the gating mechanism and the depth-wise convolution to develop an **Efficient Feed Forward (EFF)** layer that follow the $\text{conv } 1 \times 1 \rightarrow \text{GELU} \rightarrow \text{conv } 1 \times 1$ flow, which operates similarly to MLPs in Transformers, while requiring fewer parameters.

4.4 Retinex-SS2D Layer

The detailed illustration of Retinex-SS2D layer is shown as Fig. 3. We first conduct feature fusion for input feature \mathbf{F}_{in} and Retinex guidance feature \mathbf{F}_c by linear operation, depth-wise convolution, element-wisely multiplication, and SiLU operation. Subsequently, the fused feature \mathbf{F}_f is fed into our proposed **Feature-Aware 2D Selective State-space (FA-SS2D)** mechanism to capture dynamic long-range dependencies and achieve adaptive spatial aggregation. Besides, a gating signal \mathbf{G}_s and a linear operation is utilized to obtain the aggregated feature \mathbf{F}_g .

Feature-Aware 2D Selective State-space Mechanism The standard Selective State-space Model (S6) achieves outstanding performance on sequence modeling, especially for NLP task that involves temporal sequence. However, significant challenges arise when applying S6 to 2D image. To better modeling the spatial information in 2D images, several interesting works propose multiple scan strategies to unfold image patches into 1D sequences. For example, [27] introduces cross-scan strategy that generate four sequences along four distinct traversal paths, and each sequence is processed by a separate S6 operation. However, such strategy incredibly increase the computational demands, which contradicts the inherently high efficiency and low computational requirements of S6. Furthermore, these techniques only involve simple scanning of images across different directions, which results in a substantial separation of local textures and global structures in some sequences. This separation, to some extent, impairs the S6 framework’s modeling ability for images.

The deficiencies in the existing scanning approach drive us to reassess how S6 can be more effectively utilized for 2D images. As described in Eq. 2, for each token in a sequence, the output $y(t)$ depends on its input $x(t)$ and previous inputs $\{x(1), x(2), \dots, x(t-1)\}$. This mechanism requires the 1D sequences transformed from 2D image to meet the following two criteria to ensure excellent performance: (1) The sequence should prioritize the most critical feature regions at the beginning, while relegating less significant information to the end. (2) Spatially adjacent features should be

Methods	ME Dataset [1]						SICE Dataset [5]					
	Under-exposed		Over-exposed		Average		Under-exposed		Over-exposed		Average	
	PSNR↑	SSIM↑	PSNR↑	SSIM↑	PSNR↑	SSIM↑	PSNR↑	SSIM↑	PSNR↑	SSIM↑	PSNR↑	SSIM↑
ZeroDCE [16] CVPR'20	14.55	0.589	10.40	0.5142	12.06	0.544	16.92	0.633	7.11	0.429	12.02	0.531
RUAS [24] CVPR'21	13.43	0.681	6.39	0.466	9.20	0.552	16.63	0.559	4.54	0.320	10.59	0.439
URetinexNet [37] CVPR'22	13.85	0.737	9.81	0.673	11.42	0.699	17.39	0.645	7.40	0.454	12.40	0.550
KinD [44] MM'19	15.51	0.761	11.66	0.730	13.20	0.742	13.43	0.484	7.85	0.478	10.64	0.481
LLFlow* [34] AAAI'22	22.35	0.858	22.46	0.863	22.42	0.861	21.45	<u>0.679</u>	20.29	0.671	20.87	0.675
LLFlow-SKF* [38] CVPR'23	22.58	0.859	22.72	0.865	22.66	0.863	21.61	0.671	<u>20.55</u>	0.695	21.08	0.683
DRBN [40] CVPR'20	19.74	0.829	19.37	0.832	19.52	0.831	17.96	0.677	17.33	0.683	17.65	0.680
DRBN+ERL [21] CVPR'23	19.91	0.831	19.60	0.838	19.73	0.836	18.09	0.674	17.93	0.687	18.01	0.680
FECNet [20] ECCV'22	22.96	0.860	23.22	0.875	23.12	0.869	22.01	0.674	19.91	<u>0.696</u>	20.96	<u>0.685</u>
FECNet+ERL [21] CVPR'23	23.10	<u>0.864</u>	23.18	<u>0.876</u>	23.15	<u>0.871</u>	<u>22.35</u>	0.667	20.10	0.689	<u>21.22</u>	0.678
Retiformer* [6] ICCV'23	22.77	0.862	22.24	0.860	22.45	0.861	22.15	0.665	20.21	0.669	21.18	0.667
LACT [4] ICCV'23	<u>23.49</u>	0.862	<u>23.68</u>	0.872	<u>23.57</u>	0.869	-	-	-	-	-	-
Ours	23.64	0.875	23.84	0.882	23.76	0.879	22.87	0.745	21.23	0.727	22.05	0.736

Table 1: Quantitative comparisons of different methods on multi-exposure correction datasets. The best and second-best results are highlighted in **bold** and underlined, respectively. “↑” means the larger, the better. Note that we obtain these results either from the original papers, or by running the officially released pre-trained models. “*” means that original papers don’t report corresponding performance and we train their models using their officially released code.

sequenced closely to avoid significant gaps in the sequence. However, existing 2D scanning strategies fail to meet these two requirements, motivating us to propose new solutions to address this gap.

Based on these observations, we introduce an efficient Feature-Aware 2D Selective State-space (FA-SS2D) mechanism, as shown in Fig. 3. Firstly, we develop a deformable feature aggregation operation modulated by Retinex information. Specifically, Deformable Convolution (DCN) [48, 9] is adopted to capture dynamic long range dependencies of the fused feature \mathbf{F}_f . For example, when DCN is applied to the token delineated by the red frame in \mathbf{F}_f of Fig. 3, its receptive field is an irregular kernel and the activated tokens are outlined in blue. More importantly, when the red frame is sliding across the feature map, the irregular kernel varies and we record which tokens are activated. After this process, we obtain the total activation number and calculate the average activation frequency for each token. Therefore, we can obtain an activation response map shown in \mathbf{F}_d of Fig. 3, where tokens with higher activation frequency represent important features. Specifically, relatively brighter areas in under-exposed images or relatively normally exposed areas in over-exposed images contain important features and exhibit a large activation response. Based on the obtained activation response map, we propose a feature-aware scanning strategy. Different from “direction-sensitive” scanning method [27], our feature-aware strategy ranks tokens by their activation frequency and place tokens with higher frequencies at the start of the sequence. Therefore, our generated sequence effectively meets Mamba’s requirements, thereby maximizing its modeling capabilities for vision data.

4.5 Loss Functions and Constraints

In this work, we adopt the one-stage strategy to train our proposed ECMamba network, which means that the \mathcal{E} , \mathcal{M}_R , and \mathcal{M}_L are optimized simultaneously. Our ultimate training objective is to approximate \mathbf{L}_{out} to \mathbf{I}_{GT} , and we also integrate several constraints on $\bar{\mathbf{L}}$, $\bar{\mathbf{R}}$, and \mathbf{R}_{out} to achieve stable training. Therefore, our complete optimize strategy is shown as below:

$$\min_{\mathcal{E}, \mathcal{M}_R, \mathcal{M}_L} \mathcal{L}(\mathbf{I}_{out}, \mathbf{I}_{GT}) + \lambda_L \cdot \mathcal{L}_1(\bar{\mathbf{L}} \odot \mathbf{L}_{out}, \mathbf{1}) + \lambda_R \cdot \mathcal{L}_1(\bar{\mathbf{R}} \odot \mathbf{R}_{out}, \mathbf{1}) + \lambda \cdot \mathcal{L}_1(\mathbf{R}_{out}, \mathbf{I}_{GT}), \quad (8)$$

where $\mathcal{L}_1(\bar{\mathbf{L}} \odot \mathbf{L}_{out}, \mathbf{1})$ and $\mathcal{L}_1(\bar{\mathbf{R}} \odot \mathbf{R}_{out}, \mathbf{1})$ are constraints applied on $\bar{\mathbf{L}}$ and $\bar{\mathbf{R}}$, and they essentially employ a self-supervised strategy to learn $\bar{\mathbf{L}}$ and $\bar{\mathbf{R}}$. In addition, considering this optimization is inherently an ill-posed problem, we adopt $\mathcal{L}_1(\mathbf{R}_{out}, \mathbf{I}_{GT})$ to guide the optimization towards the appropriate direction. Moreover, $\mathcal{M}_L \mathcal{L}(\mathbf{I}_{out}, \mathbf{I}_{GT})$ is the primary loss function in our training process and it can be calculated by:

$$\mathcal{L}(\mathbf{I}_{out}, \mathbf{I}_{GT}) = \mathcal{L}_1(\mathbf{I}_{out}, \mathbf{I}_{GT}) + \phi_{sim} \cdot \mathcal{L}_{sim}(\mathbf{I}_{out}, \mathbf{I}_{GT}) + \phi_{per} \cdot \mathcal{L}_{per}(\mathbf{I}_{out}, \mathbf{I}_{GT}), \quad (9)$$

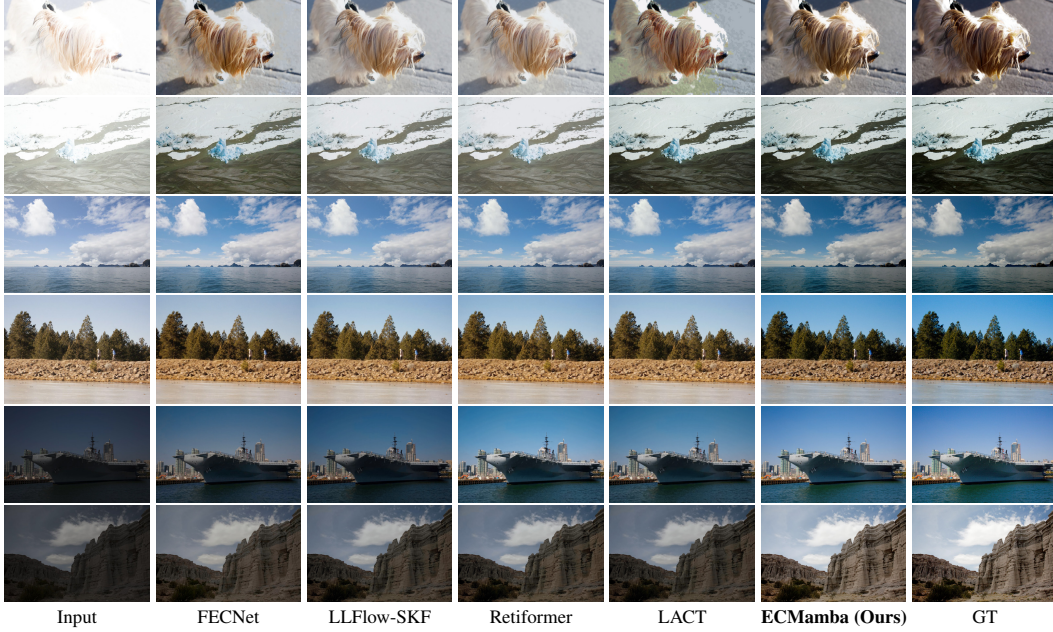


Figure 4: Visual comparison results on ME dataset. Compared to other exposure correction methods, our ECMamba excels in color preservation and structure recovery.

where \mathcal{L}_{ssim} [45] denotes the structure similarity loss and \mathcal{L}_{per} [43] represents the difference between features extracted by VGG19 [30]. The coefficients for corresponding loss functions are set as: $\phi_{ssim} = 0.2$, $\phi_{per} = 0.01$, $\lambda = 0.1$, $\lambda_R = 0.1$, and $\lambda_L = 0.1$ in this work.

5 Experiments

5.1 Experiment Settings

Datasets To evaluate the performance of our method, we conduct experiments on five prevailing datasets for multi exposure correction and under-exposure correction: ME [1], SICE [5], LOLv1 [36], LOLv2-real [41], and LOLv2-synthetic [41] datasets. Specifically, each scene in ME dataset has five exposure levels, and we regard the images with the first two exposure level as under-exposed images and the test as over-exposed images. For SICE, following FECNet [20], we select the middle exposure subset as the ground truth, and define the second and the last second exposure subset as the under-exposed and over-exposed images, respectively. For LOLv1, LOLv2-real, LOLv2-synthetic datasets, we leverage their official training and testing data for model training and evaluation.

Implementation Details We use the Adam optimizer with default parameters ($\beta_1 = 0.9$, $\beta_2 = 0.99$) to implement our model by PyTorch. The initial learning rate is set to 1×10^{-4} and then it is steadily decreased to 1×10^{-6} by the cosine annealing scheme, respectively. We utilize random flipping and rotation for data augmentation. Image pairs are cropped as 256×256 and the batch size is set to 4. The total training iterations is set to 300K for ME dataset and 150K for other benchmarks, respectively. During the evaluation, we utilize Peak Signal-to-Noise Ratio (PSNR) and Structural Similarity Index Measure (SSIM [35]) for numeric evaluation.

5.2 Performances on Multi-Exposure and Under-Exposure Correction

Quantitative Results We compare the performance of our ECMamba with current SOTA methods on multi-exposure correction datasets, and we report the quantitative results as Tab. 1. Notably, ECMamba significantly outperforms the current SOTA methods on both under-exposed and over-exposed images within ME dataset and SICE dataset. Specifically, our ECMamba excels in PSNR and SSIM, outperforming the second best method over 0.19 dB and 0.007 on ME dataset. Furthermore,

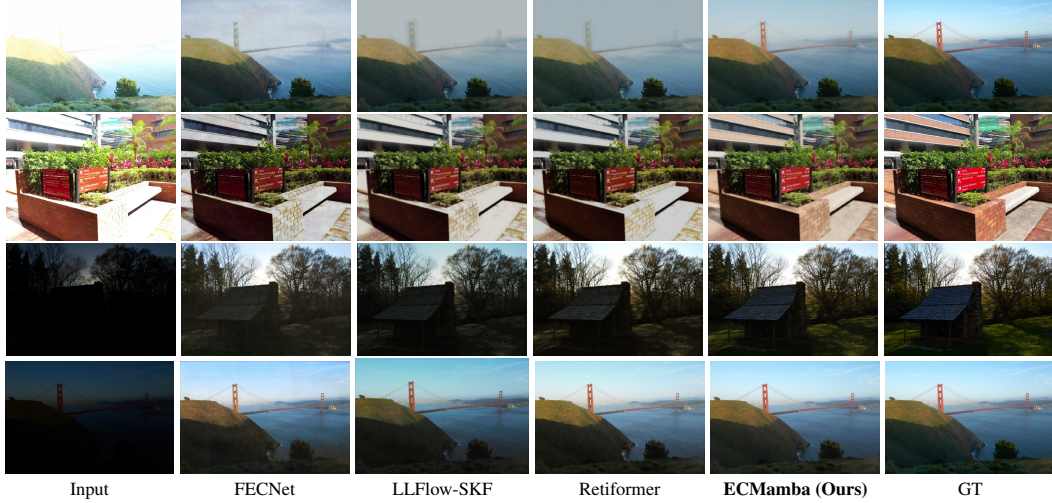


Figure 5: Visual comparisons between ECMamba and other methods on SICE dataset. Our proposed ECMamba achieves compelling visual performance both on over-exposed and under-exposed images.

Methods	LOLv1 [36]		LOLv2-real [41]		LOLv2-synthetic [41]		Param (M)↓
	PSNR↑	SSIM↑	PSNR↑	SSIM↑	PSNR↑	SSIM↑	
Zero-DCE [16] CVPR'20	14.86	0.562	18.06	0.580	-	-	0.33
RUAS [24] CVPR'21	18.23	0.720	18.37	0.723	16.55	0.652	0.003
URetinet-Net [37] CVPR'22	21.33	0.835	21.16	0.840	24.14	0.928	1.32
KinD [44] MM'19	20.86	0.790	14.74	0.641	13.29	0.578	8.02
LLFlow [34] AAAI'22	25.19	0.870	26.53	0.892	26.08	0.940	37.68
LLFlow-SKF [38] CVPR'23	<u>26.80</u>	<u>0.879</u>	<u>28.19</u>	<u>0.905</u>	<u>28.86</u>	<u>0.953</u>	39.91
DRBN [40] CVPR'20	19.39	0.817	20.29	0.831	23.22	0.927	5.27
DRBN+ERL [21] CVPR'23	19.84	0.830	-	-	-	-	-
FECNet [20] ECCV'22	22.03	0.836	20.29	0.831	23.22	0.927	0.15
FECNet+ERL [21] CVPR'23	21.08	0.829	-	-	-	-	-
Retiformer [6] ICCV'23	25.16	0.845	22.80	0.840	25.67	0.930	1.61
LACT* [4] ICCV'23	26.49	0.867	26.95	0.888	27.24	0.941	6.73
ECMamba (Ours)	27.69	0.885	29.24	0.908	29.94	0.959	1.75

Table 2: Quantitative comparisons of different methods for under-exposed correction. Notably, compared to SOTA methods, our ECMamba achieves enhanced performance on LOLv1 [36], LOLv2-real [41], and LOLv2-synthetic [41] datasets, demonstrating the effective of our proposed dual-branch Retinex-based framework and feature-aware SS2D layer.

compared to the second best performance, our improvement has increased to 0.83 dB and 0.051 on SICE dataset. Tab. 2 summarizes the quantitative comparisons between our method with current SOTA methods on on under-exposure correction. Specifically, our ECMamba outperforms the second best performance (LLFlow-SKF) by an average 1.10 dB increase on PNSR with only 4.4% parameters, revealing the impressive effectiveness and high efficiency of our proposed ECMamba. These numbers demonstrate the superior quality of our enhancement and prove the effectiveness of our proposed ECMamba and two-branch Retinex-based pipeline.

Qualitative Comparisons We present the enhanced images of different methods in Fig. 4 (ME) and Fig. 5 (SICE). Our appealing and realistic enhancement results demonstrate our model can generate images with pleasant illumination, correct color retrieval, and enhanced texture details. For example, the rich structural details of cloud patterns (row 2) mountain surface (row 4) and in Fig. 4, the well preserved bridge and its edge contours (row 1) and the vivid presentation of words in the

Methods	PSNR \uparrow	SSIM \uparrow	Param (M) \downarrow	Methods	PSNR \uparrow	SSIM \uparrow	Param (M) \downarrow
Removing \mathcal{M}_L	21.55	0.721	1.0	ViT	21.88	0.724	14.46
Removing \mathcal{M}_L^*	21.63	0.723	1.93	Retiformer	21.35	0.702	1.6
Removing \mathcal{E}	21.12	0.695	1.5	Cross-Scan Mechanism	21.69	0.716	2.1

Table 3: Ablation studies on SICE dataset and the average PSNR and SSIM are reported. *Left* is used to verify the effectiveness of the two-branch Retinex-based framework, *right* is to present the importance of our proposed ECMamba module and FA-SS2D strategy. [Key: *: When \mathcal{M}_L is removed, the hidden dimension of \mathcal{M}_R is increased to ensure its parameter number is comparable to ECMamba; ViT/Retiformer: utilized to replace our ECMamba module; Cross-Scan Mechanism: adopted to replace our FA-SS2D strategy.]

display board (row 2) in Fig. 5. In contrast, previous methods struggle to preserve color fidelity and illumination harmonization.

5.3 Ablation Study

To verify the effectiveness of our proposed ECMamba, we conduct extensive ablation experiments and report the average performance on SICE dataset.

The Contribution of Two-branch Retinex-based Framework We first remove the branch (\mathcal{M}_L), which is utilized for accurate restoration of the illumination map. Therefore, the remaining network aims to optimize \mathbf{R}_{out} to the ground truth and the performance is reported in Tab. 3, which still presents competitive performance compared to the current SOTA in Tab. 1. However, compare to our complete ECMamba, only optimizing the relectance inevitably leads to sub-optimal performance. Furthermore, we also adopt a more complicated \mathcal{M}_R , whose parameters is comparable to the original two-branch framework. However, compared to our two-branch ECMamba, this network still demonstrate poor performance. Finally, similar to other Retinex-based methods [37], we then remove the Retinex estimator \mathcal{E} and directly adopt the remaining network for exposure correction. However, as shown in Tab. 3, this adaptation largely decrease the performance of our ECMamba, indicating the importance of our analysis regarding the intermediary space (\mathbf{R}' and \mathbf{L}') in Sec. 4.1.

The Importance of Our Proposed ECMamba Module First, we replace our ECMamba module with Vision Transformer (ViT) [11] and Retiformer [6] architecture in our two-branch framework. As presented in Tab. 3, our complete ECMamba module offers impressive performance better than ViT. More importantly, ECMamba’s efficiency is comparable to Retiformer, which is a famous efficient under-exposure correction approach. Furthermore, to study the significance of our proposed Retinex-SS2D layer and FA-SS2D, we replace the Retinex-SS2D layer with a cross-scan mechanism proposed in VMamba [27]. The increased parameters and decreased performance demonstrate the superiority of our proposed Retinex-SS2D layer and FA-SS2D strategy.

6 Conclusions

We propose a new two-branch Retinex-based Mamba architecture for exposure correction. By carefully deriving Retinex theory, we propose an two-branch framework guided by Retinex information. To better balance the performance and efficiency, we introduce ECMamba as the primary restoration module with efficient Retinex-guided SS2D layer and Feature-aware scanning strategy. Extensive experiments demonstrate that our ECMamba significantly outperforms the current SOTA methods on both multi-exposure correction datasets and under-exposure correction datasets. We recognize that our work, while pioneering in certain aspects, also highlights avenues for future investigation. For example, similar to other methods, ECMamba struggles to deliver satisfactory results in scenarios involving extreme exposure cases (extremely dark or over-exposed environments) due to the extensive information loss inherent in degraded images. Essentially, directing recovery from severely degraded images is challenging, but recent advances in image restoration have utilized generative priors to infer the degraded details, and achieve favorable results. In the future, we plan to integrate Mamba with generative priors to effectively alleviate the performance drop on extreme exposure cases.

References

- [1] Mahmoud Afifi, Konstantinos G Derpanis, Bjorn Ommer, and Michael S Brown. Learning multi-scale photo exposure correction. In *Proceedings of the IEEE Conference on Computer Vision and Pattern Recognition (CVPR)*, 2021.
- [2] Codruta O. Ancuti, Cosmin Ancuti, Florin-Alexandru Vasluianu, Radu Timofte, et al. Ntire 2024 dense and nonhomogeneous dehazing challenge report. In *Proceedings of the IEEE Conference on Computer Vision and Pattern Recognition Workshops (CVPR Workshops)*, 2024.
- [3] Codruta O. Ancuti, Cosmin Ancuti, Florin-Alexandru Vasluianu, Radu Timofte, Han Zhou, Wei Dong, et al. NTIRE: 2023 hr nonhomogeneous dehazing challenge report. In *Proceedings of the IEEE Conference on Computer Vision and Pattern Recognition Workshops (CVPR Workshops)*, 2023.
- [4] Jong-Hyeon Baek, DaeHyun Kim, Su-Min Choi, Hyo-jun Lee, Hanul Kim, and Yeong Jun Koh. Luminance-aware color transform for multiple exposure correction. In *Proceedings of the IEEE International Conference on Computer Vision (ICCV)*, 2023.
- [5] Jianrui Cai, Shuhang Gu, and Lei Zhang. Learning a deep single image contrast enhancer from multi-exposure images. In *IEEE Transactions on Image Processing (TIP)*, 2018.
- [6] Yuanhao Cai, Hao Bian, Jing Lin, Haoqian Wang, Radu Timofte, and Yulun Zhang. Retinexformer: One-stage retinex-based transformer for low-light image enhancement. In *Proceedings of the IEEE International Conference on Computer Vision (ICCV)*, 2023.
- [7] Van der Maaten L and Hinton G. Visualizing data using t-sne. In *Journal of machine learning research*, 2008.
- [8] Wei Dong, Han Zhou, Yuqiong Tian, Jingke Sun, Xiaohong Liu, Guangtao Zhai, and Jun Chen. ShadowRefiner: Towards mask-free shadow removal via fast fourier transformer. In *Proceedings of the IEEE Conference on Computer Vision and Pattern Recognition Workshops (CVPR Workshops)*, 2024.
- [9] Wei Dong, Han Zhou, Ruiyi Wang, Xiaohong Liu, Guangtao Zhai, and Jun Chen. DehazeDCT: Towards effective non-homogeneous dehazing via deformable convolutional transformer. In *Proceedings of the IEEE Conference on Computer Vision and Pattern Recognition Workshops (CVPR Workshops)*, 2024.
- [10] Wei Dong, Han Zhou, and Dong Xu. A new sclera segmentation and vessels extraction method for sclera recognition. In *2018 10th International Conference on Communication Software and Networks (ICCSN)*, 2018.
- [11] Alexey Dosovitskiy, Lucas Beyer, Alexander Kolesnikov, Dirk Weissenborn, Xiaohua Zhai, Thomas Unterthiner, Mostafa Dehghani, Matthias Minderer, Georg Heigold, Sylvain Gelly, et al. An image is worth 16x16 words: Transformers for image recognition at scale. In *Proceedings of the International Conference on Learning Representations (ICLR)*, 2020.
- [12] Kang Fu, Yicong Peng, Zicheng Zhang, Qihang Xu, Xiaohong Liu, Jia Wang, and Guangtao Zhai. Attentionlut: Attention fusion-based canonical polyadic lut for real-time image enhancement. *arXiv preprint arXiv:2401.01569*, 2024.
- [13] Xueyang Fu, Delu Zeng, Yue Huang, Xiao-Ping Zhang, and Xinghao Ding. A weighted variational model for simultaneous reflectance and illumination estimation. In *Proceedings of the IEEE Conference on Computer Vision and Pattern Recognition (CVPR)*, 2016.
- [14] Albert Gu and Tri Dao. Mamba: Linear-time sequence modeling with selective state spaces. *arXiv preprint arXiv:2312.00752*, 2023.
- [15] Albert Gu, Karan Goel, and Christopher Ré. Efficiently modeling long sequences with structured state spaces. In *Proceedings of the International Conference on Learning Representations (ICLR)*, 2022.
- [16] Chunle Guo, Chongyi Li, Jichang Guo, Chen Change Loy, Junhui Hou, Sam Kwong, and Runmin Cong. Zero-reference deep curve estimation for low-light image enhancement. In *Proceedings of the IEEE Conference on Computer Vision and Pattern Recognition (CVPR)*, 2020.
- [17] Hang Guo, Jinmin Li, Tao Dai, Zhihao Ouyang, Xudong Ren, and Shu-Tao Xia. Mambair: A simple baseline for image restoration with state-space model. In *Proceedings of the European Conference on Computer Vision (ECCV)*, 2024.
- [18] Xiaojie Guo, Yu Li, and Haibin Ling. Lime: Low-light image enhancement via illumination map estimation. In *IEEE Transactions on Image Processing (TIP)*, 2016.

- [19] Jie Huang, Yajing Liu, Xueyang Fu, Man Zhou, Yang Wang, Feng Zhao, and Zhiwei Xiong. Exposure normalization and compensation for multiple-exposure correction. In *Proceedings of the IEEE Conference on Computer Vision and Pattern Recognition (CVPR)*, 2022.
- [20] Jie Huang, Yajing Liu, Feng Zhao, Keyu Yan, Jinghao Zhang, Yukun Huang, Man Zhou, and Zhiwei Xiong. Deep fourier-based exposure correction with spatial-frequency interaction. In *Proceedings of the European Conference on Computer Vision (ECCV)*, 2022.
- [21] Jie Huang, Feng Zhao, Man Zhou, Jie Xiao, Naishan Zheng, Kaiwen Zheng, and Zhiwei Xiong. Learning sample relationship for exposure correction. In *Proceedings of the IEEE Conference on Computer Vision and Pattern Recognition (CVPR)*, 2023.
- [22] Edwin H Land. The retinex theory of color vision. *Scientific american*, 1977.
- [23] Wenhao Li, Guangyang Wu, Wenyi Wang, Peiran Ren, and Xiaohong Liu. Fastllve: Real-time low-light video enhancement with intensity-aware lookup table. In *Proceedings of the ACM Conference on Multimedia (MM)*, 2023.
- [24] Risheng Liu, Long Ma, Jiaao Zhang, Xin Fan, and Zhongxuan Luo. Retinex-inspired unrolling with cooperative prior architecture search for low-light image enhancement. In *Proceedings of the IEEE Conference on Computer Vision and Pattern Recognition (CVPR)*, 2021.
- [25] Xiaohong Liu, Yongrui Ma, Zhihao Shi, and Jun Chen. Griddehazenet: Attention based multi-scale network for image dehazing. In *Proceedings of the IEEE International Conference on Computer Vision (ICCV)*, 2019.
- [26] Xiaohong Liu, Zhihao Shi, Zijun Wu, Jun Chen, and Guangtao Zhai. Griddehazenet+: An enhanced multi-scale network with intra-task knowledge transfer for single image dehazing. *IEEE Transactions on Intelligent Transportation Systems*, 2022.
- [27] Yue Liu, Yunjie Tian, Yuzhong Zhao, Hongtian Yu, Lingxi Xie, Yaowei Wang, Qixiang Ye, and Yunfan Liu. Vmamba: Visual state space model. *arXiv preprint arXiv:2401.10166*, 2024.
- [28] Zhuang Liu, Hanzi Mao, Chao-Yuan Wu, Christoph Feichtenhofer, Trevor Darrell, and Saining Xie. A convnet for the 2020s. *Proceedings of the IEEE/CVF Conference on Computer Vision and Pattern Recognition (CVPR)*, 2022.
- [29] Yuan Shi, Bin Xia, Xiaoyu Jin, Xing Wang, Tianyu Zhao, Xin Xia, Xuefeng Xiao, and Wenming Yang. Vmambair: Visual state space model for image restoration. *arXiv preprint arXiv:2403.11423*, 2024.
- [30] Karen Simonyan and Andrew Zisserman. Very deep convolutional networks for large-scale image recognition. In *Proceedings of the International Conference on Learning Representations (ICLR)*, 2015.
- [31] V. A. Sindagi, P. Oza, R. Yasarla, and V.M. Patel. Prior-based domain adaptive object detection for hazy and rainy conditions. In *Proceedings of the European Conference on Computer Vision (ECCV)*, 2020.
- [32] Florin-Alexandru Vasluianu, Tim Seizinger, Zhuyun Zhou, Zongwei Wu, Cailian Chen, Radu Timofte, et al. NTIRE 2024 image shadow removal challenge report. In *Proceedings of the IEEE Conference on Computer Vision and Pattern Recognition Workshops (CVPR Workshops)*, 2024.
- [33] Ruixing Wang, Qing Zhang, Chi-Wing Fu, Xiaoyong Shen, Wei-Shi Zheng, and Jiaya Jia. Underexposed photo enhancement using deep illumination estimation. In *Proceedings of the IEEE Conference on Computer Vision and Pattern Recognition (CVPR)*, 2019.
- [34] Yufei Wang, Renjie Wan, Wenhan Yang, Haoliang Li, Lap-Pui Chau, and Alex Kot. Low-light image enhancement with normalizing flow. In *Proceedings of the AAAI Conference on Artificial Intelligence (AAAI)*, 2022.
- [35] Zhou Wang, Alan C Bovik, Hamid R Sheikh, and Eero P Simoncelli. Image quality assessment: From error visibility to structural similarity. In *IEEE Transactions on Image Processing (TIP)*, 2004.
- [36] Chen Wei, Wenjing Wang, Wenhan Yang, and Jiaying Liu. Deep retinex decomposition for low-light enhancement. In *Proceedings of the Conference on British Machine Vision Conference (BMVC)*, 2018.
- [37] Wenhui Wu, Jian Weng, Pingping Zhang, Xu Wang, Wenhan Yang, and Jianmin Jiang. Uretinex-net: Retinex-based deep unfolding network for low-light image enhancement. In *Proceedings of the IEEE Conference on Computer Vision and Pattern Recognition (CVPR)*, 2022.

- [38] Yuhui Wu, Chen Pan, Guoqing Wang, Yang Yang, Jiwei Wei, Chongyi Li, and Heng Tao Shen. Learning semantic-aware knowledge guidance for low-light image enhancement. In *Proceedings of the IEEE Conference on Computer Vision and Pattern Recognition (CVPR)*, 2023.
- [39] Dong Xu, Wei Dong, and Han Zhou. Sclera recognition based on efficient sclera segmentation and significant vessel matching. In *The Computer Journal*, 2022.
- [40] Wenhan Yang, Shiqi Wang, Yuming Fang, Yue Wang, and Jiaying Liu. From fidelity to perceptual quality: A semi-supervised approach for low-light image enhancement. In *Proceedings of the IEEE/CVF Conference on Computer Vision and Pattern Recognition*, pages 3063–3072, 2020.
- [41] Wenhan Yang, Wenjing Wang, Haofeng Huang, Shiqi Wang, and Jiaying Liu. Sparse gradient regularized deep retinex network for robust low-light image enhancement. In *IEEE Transactions on Image Processing (TIP)*, 2021.
- [42] Xiangyu Yin, Xiaohong Liu, and Huan Liu. Fmsnet: Underwater image restoration by learning from a synthesized dataset. In *International Conference on Artificial Neural Networks (ICANN)*, 2019.
- [43] Richard Zhang, Phillip Isola, A.A. Efros, Eli Shechtman, and Oliver Wang. The unreasonable effectiveness of deep features as a perceptual metric. In *Proceedings of the IEEE Conference on Computer Vision and Pattern Recognition (CVPR)*, 2018.
- [44] Yonghua Zhang, Jiawan Zhang, and Xiaojie Guo. Kindling the darkness: A practical low-light image enhancer. In *Proceedings of the ACM Conference on Multimedia (MM)*, 2019.
- [45] Han Zhou, Wei Dong, Yangyi Liu, and Jun Chen. Breaking through the haze: An advanced non-homogeneous dehazing method based on fast fourier convolution and convnext. In *Proceedings of the IEEE Conference on Computer Vision and Pattern Recognition Workshops (CVPR Workshops)*, 2023.
- [46] Han Zhou, Wei Dong, Yulun Zhang, Xiaohong Liu, and Jun Chen. GLARE: low light image enhancement via generative latent feature based codebook retrieval. In *Proceedings of the European Conference on Computer Vision (ECCV)*, 2024.
- [47] Lianghui Zhu, Bencheng Liao, Qian Zhang, Xinlong Wang, Wenyu Liu, and Xinggang Wang. Vision mamba: Efficient visual representation learning with bidirectional state space model. In *Proceedings of the International Conference on Machine Learning (ICML)*, 2024.
- [48] Xizhou Zhu, Han Hu, Stephen Lin, and Jifeng Dai. Deformable convnets v2: More deformable, better results. In *Proceedings of the IEEE Conference on Computer Vision and Pattern Recognition (CVPR)*, 2019.